A p53 Oscillator Model of DNA Break Repair Control

Vijay Chickarmane, Ali Nadim, Animesh Ray and Herbert M. Sauro [*]

Keck Graduate Institute, 535 Watson Dr, Claremont, CA 91711

October 4, 2005

Abstract

The transcription factor p53 is an important regulator of cell fate. Mutations in p53 gene are associated with many cancers. In response to signals such as DNA damage, p53 controls the transcription of a series of genes that cause cell cycle arrest during which DNA damage is repaired, or triggers programmed cell death that eliminates possibly cancerous cells wherein DNA damage might have remained unrepaired. Previous experiments showed oscillations in p53 level in response to DNA damage, but the mechanism of oscillation remained unclear. Here we examine a model where the concentrations of p53 isoforms are regulated by Mdm22, Arf, Siah, and β-catenin. The extent of DNA damage is signalled through the switch-like activity of a DNA damage sensor, the DNA-dependent protein kinase Atm. This switch is responsible for initiating and terminating oscillations in p53 concentration. The strength of the DNA damage signal modulates the number of oscillatory waves of p53 and Mdm22 but not the frequency or amplitude of oscillations–a result that recapitulates experimental findings. A critical finding was that the phosphorylated form of Nbs11, a member of the DNA break repair complex Mre11-Rad50-Nbs11 (MRN), must augment the activity of

[*]Corresponding Author :Herbert M Sauro, Keck Graduate Institute, 535 Watson Drive, Claremont, CA 91711, Phone: (909) 607 0377, Fax: (909) 607 8086, E-mail: hsauro@kgi.edu

1

Atm kinase. While there is in vitro support for this assumption, this activity appears essential for p53 dynamics. The model provides several predictions concerning, among others, degradation of the phosphorylated form of p53, the rate of DNA repair as a function of DNA damage, the sensitivity of p53 oscillation to transcription rates of SIAH, β-CATENIN and ARF, and the hysteretic behavior of active Atm kinase levels with respect to the DNA damage signal.

The p53 protein is a transcription factor that is present in most higher eukaryotes. It regulates the expression of a series of genes that mediates cell cycle arrest and apoptosis in response to DNA damage and extracellular signals [1]. p53 gene is often mutated in tumor cells [2, 3]. It is necessary for the elimination of potentially cancerous cells by triggering cell death [4] and is thought to be a major tumor suppressor gene [5, 6]. p53 protein is subject to a series of post translational modifications that modulate its kinase activity [1]. A simple view is that p53 is present in at least two major forms, an unphosphorylated form that is thought to be inactive as a transcription factor, which is rapidly turned over by proteolysis and a more stable phosphorylated form. Phosphorylation occurs at a number of amino acid residues on the protein by the activity of protein kinases, and the phosphate groups are in turn removed by the activity of several phosphatases that are dynamically associated with p53.

A phosphorylated form of p53, p53-P, is the active transcription factor that binds to a number of target DNA sites that regulate the expression of several genes involved in cell cycle checkpoint arrest and programmed cell death, respectively [7]. Additionally, p53-P induces transcription of the gene *p53AIP1*, whose product in the cytoplasm leads to the release of cytochrome c protein from mitochondria, which in turn activates programmed cell death directly by activating the cytoplasmic protease cascade [8].

Ionizing radiation causes DNA double strand breaks that triggers the binding of the sensor protein kinase Atm [9]to the nascent DNA ends [10]. DNA binding triggers the kinase activity of Atm, which then phosphorylates preexisting p53 proteins to p53-P [11, 12]. Unphosphorylated p53 is the substrate of Mdm2, a ubiquitin E3 ligase [13]. Once ubiquitinated, p53-P protein is proteolytically degraded by the proteosome complex. By contrast, p53-P is more resistant to ubiquitination, therefore is more stable. Hence Atm activation leads to the accumulation of p53-P. Nuclear localized p53-P binds to the regulatory sequences of several

genes among which MDM2 is one. This binding increases the transcription of MDM2 gene. Thus an increase in p53-P concentration in the nucleus increases the synthesis of Mdm2 RNA and protein. The increase in Mdm2 protein concentration is expected to destabilize any remaining unphosphorylated p53 by ubiquitination and proteasome-mediated degradation. Using this negative feedback, p53 regulates its own concentration in the cell [4].

DNA double strand breaks induced by ionizing radiation are thought to cause certain topological changes in the chromatin structure such that the inactive Atm kinase homodimer molecules associated with the chromatin become activated [12]. One of the two Atm kinase subunits phosphorylates the other at the serine-1081 residue leading to reciprocal phosphorylation of the two Atm kinase subunits. The dimer is thought to dissociate and the phosphorylated monomers have three central functions: First, phosphorylation of nuclear-localized p53 to p53-P; second, phosphorylation of Brca1 and Brca2 proteins to activate cell-cycle checkpoint arrest and blockage of DNA replication fork movement; and third, recruitment of the MRN (Mre11-Rad50-Nbs1) DNA repair complex to the nascent DNA ends by protein-protein interaction while simultaneously activating the function of the MRN complex by phosphorylating Nbs1 to Nbs1-P [14, 15]. The activated MRN complex begins to repair the broken DNA either by nonhomologous end joining or by recombinational repair using the unbroken homolog as a template. p53-P directly recruits RAD51 protein at the MRN complex by protein-protein interactions [16] where RAD51 constrains the recombinational repair of DNA by the non-crossover mode. This mode of DNA repair protects the genome from somatic aneuploidy that is often an early event during cancer formation [17]. Yet another effect of p53-P is that it slowly accumulates in the cytoplasm where it causes the mitochondrial membrane to leak cytochrome c protein fragments [8]. Accumulating cytochrome c in the cytoplasm is ultimately responsible for inactivating the anti-apoptotic proteins Bcl2/Bax, which leads to apoptosis. However, the relative rates of cytoplasmic p53-P accumulation and its nuclear effects in DNA repair determine the fate of the cell: repair of DNA damage or death. Thus, the levels of p53 protein and its phosphorylated form

are crucial determinants of cell fate.

Recently Lahav et al. [18] measured intracellular concentration of total p53 and Mdm2 proteins by fusing their coding sequences to fluorescent reporter domains. Examination of single mouse cells following treatment with ionizing radiation that produces DNA double stranded breaks (DSB) revealed that p53 and Mdm2 protein concentrations in singles cells oscillate in response to DNA damage. The period and the amplitude of these oscillations remained constant over a range of radiation doses, but the number of pulses was proportional to the radiation dose. Lahav et al. [18] proposed that the system behaves as a "digital oscillator".

In response, Tyson [19] proposed that following DNA damage the steady state p53 concentration passes through a Hopf bifurcation [20, 21] and begins to oscillate. Once the damage is corrected the system is pulled back from the oscillatory region to its original steady state. This idea was further expanded in an explicit model that assumed regulation of p53 degradation by Mdm2 and p53 as a transcription factor for Mdm2 RNA synthesis [22]. A crucial aspect of this model is a positive feedback loop by which p53 inhibits the nuclear localization of Mdm2 into the nucleus [23], thereby increasing the p53 levels.

Another approach to modeling the p53 dynamics makes explicit use of delays in the system corresponding to the time it takes for transcription and translation of the Mdm2 protein [24] [1]. Oscillations are possible by including a sufficiently long delay, as for example in the case of a hypothetical intermediate step introduced by Alon et al. [25].

While previous modeling approaches explored the conditions that could in principle generate oscillations in p53 and Mdm2 levels, these models did not specifically address explicit molecular mechanisms of DNA break repair or control of p53 activity. Here, in a significant departure from previous studies, we explicitly model changes in unphosphorylated and phosphorylated versions of p53 in response to DNA damage. We ignore the nuclear transport of p53 because the time-scale of nuclear localization (minutes) is fast compared to that of the observed oscillatory dynamics (hours). We include in the model a specific pathway, that

---

[1]Tiana, G., Jensen, M.H., & Sneppen, K., (2002) *arXiv:cond-mat/0207236v1*

includes the regulation of Mdm2 through p53-P using Arf(p19), β-catenin, and Siah [4]. We also explicitly model the activation of the Atm kinase, which phosphorylates p53 as a switch.

The model reproduces the experimentally observed oscillatory dynamics in p53 and Mdm2 protein concentrations and generates a range of novel molecular predictions that can be tested by future experiments. These predictions include: the expected degradation profile of p53-P, the rate at which DNA is repaired is proportional to the degree of DNA damage, the sensitivity of p53-P oscillations to the transcription rates of several genes including SIAH, β-CATENIN and ARF, and, finally, specific predictions on the hysteretic behavior of the Atm kinase switch.

Methods

All simulations were carried out using the Systems Biology Workbench (SBW/BioSPICE) tools [26]: the network designer, JDesigner, the simulation engine Jarnac [27]. Bifurcation diagrams were computed using SBW with an interface to MATLAB [28], and a bifurcation discovery tool [29]. Bifurcation plots were also computed and cross checked using Oscill8 [2], an interactive bifurcation software package which is linked to AUTO [30], and SBW [26]. In all our simulations the species concentrations are regarded as dimensionless, whereas the kinetic constants have dimensions of inverse time, with dimensionless Michaelis-Menten constants. All models are available as standard SBML or Jarnac scripts. In the sensitivity analysis of a network, the control coefficients C_j^i are defined as, $C_j^i = \frac{p_j}{S_i}\frac{\partial S_i}{\partial p_j}$, where S_i, p_j are the species, and the parameters respectively.

---

[2]http://sourceforge.net/projects/oscill8

Results

The Model

We modularize the network [31] into three distinct dynamically different pieces: a switch describing the Atm kinase, a subnetwork that describes the DNA damage repair, and an oscillator that includes p53 and Mdm2 (Fig 1). DNA damage turns on the Atm kinase switch which then turns on the oscillator. The oscillations activate and maintain the repair process. As the damage is corrected, the switch is shut off; this in turn switches off the oscillator (see Fig 6).

Module A: DNA Repair

We assume that when DNA is damaged a signal S_D, which is proportional to the damage, is generated. Repair of DNA breaks decreases S_D. In reality, S_D is equivalent to the number of nascent double stranded DNA ends created due to the interaction of ionizing radiation with DNA. In response to the DNA damage, Atm is phosphorylated to Atm-P, and the activated Atm-P kinase in turn phosphorylates a host of target proteins, including Nbs1, Brca1, Brca2 and p53. Brca1 and Brca2 block DNA replication and cell cycle. The phosphorylated form Nbs1-P recruits Mre11 and Rad50, and the complex of three proteins (the MRN complex) binds the broken DNA to initiate repair-recombination. Hence the repair process begins once concentrations of Atm-P kinase, Nbs1 kinase and p53-P begin to grow. The rate of repair is thus described by

$$\frac{d[S_D]}{dt} = -\alpha_D[\text{p53-P}][\text{Nbs1-P}][\text{Atm-P}][S_D], \tag{1}$$

where $\alpha_D = 2 \times 10^{-4}$, is a rate constant of the decay in damage signal, which can be calculated by measuring the change in the number of DNA ends per genome. The bracketed variables

refer to the concentration of the various species, in dimensionless form. For simplicity we assume that all double strand break (DSB) repair is dependent on p53; this is clearly untrue because more error prone p53 independent repair pathways exist.

Module B: Atm Switch

Atm proteins are normally sequestered in the form of dimers/multimers, and are thought to undergo autophosphorylation [12, 32]. A class of phosphatases, PP-2A, are known to de-phosphorylate Atm-P [33]. When a DSB occurs, two events happen very quickly. The first is that the phosphatases dissociate from Atm multimers and this results in an increased phosphorylation rate, and the second is that the Atm dimers dissociate to activated monomers. It has been hypothesized that "turning off" the suppressive effect of the phosphatases on the autophosphorylation of Atm allows rapid signal transduction of the DNA damage signal [33]. Upon DNA damage, Atm-P accumulates rapidly in the nucleus [12]. We assume that the effect of ionizing radiation is to reduce the ability of the phosphatases to bind to Atm. This reduction in the phosphatase activity following DNA damage could be thought to occur due to competition among Atm-P and the signal S_D to bind to the phosphatases. However, we do not explicitly model the competitive inhibition but use a mathematical rate law that is derived from such an assumption. It is known that Atm-P phosphorylates Nbs1, which is part of the MRN complex, and that the MRN complex further increases the activity of Atm [14, 15]. We take this as a cue to modelling the interaction between Atm and Nbs1 as a positive feedback system. As such, active Atm (i.e. phosphorylated Atm) will activate Nbs1 in the MRN complex (through phosphorylation), leading to further activity in Atm. This explains why Atm-P levels increase rapidly in the cell upon DNA damage. Thus, Nbs1-P positively regulates (thick dotted line in Fig. 1, Module B) activity of Atm by causing its phosphorylation. Alternatively, one can regard this effect to be due to a further activation of Atm-P by Nbs1-P; for simplicity we do not introduce a new variable for the "active" form of Atm-P. We do not know the exact process by which this may occur, but

find that such a process is required by the model to be able to predict the experimental observations of the p53 dynamics (see later).

Referring to Fig. 1, Module B, the equations (see supplementary materials for reaction scheme) for Atm, and Nbs1 are,

$$
\begin{aligned}
\frac{d[\text{Atm-P}]}{dt} &= \frac{[\text{Atm}][\text{Nbs1-P}]}{k_1 + [\text{Atm}]} + \alpha - \frac{[\text{Atm-P}]}{k_2 + [\text{Atm-P}]}\left(\frac{\alpha_s}{k_0 + [S_D]}\right), \\
\frac{d[\text{Nbs1-P}]}{dt} &= \frac{[\text{Nbs1}][\text{Atm-P}]}{k_4 + [\text{Nbs1}]} + \beta - \frac{[\text{Nbs1-P}]}{k_3 + [\text{Nbs1-P}]}
\end{aligned}
\tag{2}
$$

where the assumption of the positive feedback (marked as the dotted line in Fig. 1 Module B) is given by the first term in the rate law for Atm-P. α, β, are basal rates of phosphorylation due to stochastic fluctuations in Atm and Nbs1 kinase activities, respectively. In the above equations, the rate constants are in units of inverse time, α_s is a scaling parameter, and the Michaelis-Menten constants $(k_1, k_2, k_3, k_4, k_0)$ are in dimensionless units. The parameter values for these equations are reported in supplementary materials.

Using the above equations the steady state values of Atm-P reached by the system as a function of the DNA damage, S_D, was computed in Fig. 2A. The system shows bistability, i.e. two possible steady states for a range of S_D. For large values of damage $(S_D > 2.7)$, Atm-P $= 1$, and the switch is in the **ON** state. As the damage is corrected, and drops below $\simeq 0.08$, the switch is turned **OFF**. The plot for Nbs1-P is very similar, and this is due to the nature of the positive feedbacks that Atm and Nbs1 have on each other. There are several examples where positive feedback can give rise to bistable, switch-like, behavior [34, 35, 36]. The system can therefore move between two states, a low state defined by low values of Atm and Nbs1, and a high state defined by high values of Atm-P and Nbs1-P. As shown in Fig. 2B, as the damage decreases below $\simeq 0.08$, the switch is turned to the **OFF** state, and

9

Atm-P levels drop off rapidly.

In the present model the positive feedback between Atm-P and Nbs1-P has significant effects on the dynamics of the integrated system. Neglecting the positive feedback still gives a quick response in Atm-P levels to DNA damage, but as the DNA is repaired, the Atm-P levels do not fall off abruptly, but gradually decrease (supplementary materials). For the integrated model to produce the observed [18] results that describe the experimental observations it is necessary to have a switch-like behavior in Atm-P levels that in turn requires the stated positive feedback.

Module C: p53 Oscillator:

To determine whether the known regulatory network involving p53 and Mdm2 is sufficient to reproduce their observed dynamics, we proceed as follows. The central oscillator is composed of the negative feedback of Mdm2 on p53 stability through ubiquitination, and the dependence of Mdm2 expression on p53-P. The latter is produced by Atm-P in response to the DNA damage. The dephosphorylation of p53-P is described by a Michaelis-Menten scheme, and is assumed to occur at a very small rate compared to the phosphorylation rate. We assume small first order degradation rates for both p53 and p53-P. p53-P is a more stable form of p53, and hence its rate of degradation is smaller than the degradation rate for p53. We model the degradation of p53-P as a function of Mdm2; this is done to match qualitatively the simulation results of our model to the experimental results (see below). Furthermore, p53 indirectly regulates the amount of Mdm2 that is available for binding to p53 through the former's transcription factor activity on the SIAH gene [4]. The Siah protein is a ubiquitin ligase, and enhances the degradation of β-catenin. β-catenin, which is produced constitutively, regulates the transcription of the Arf gene. The Arf protein binds to Mdm2, sequestering the latter from its substrates and also promoting the latter's degrada-

tion such that increasing concentration of Arf should increase the p53 level [3]. The following differential equations describe the dynamics of module C in Fig. 1, and were generated automatically by SBW from SBML [26].

$$
\begin{aligned}
\frac{d[\text{p53}]}{dt} &= c_0 - \frac{[\text{Atm-P}][\text{p53}]}{k_p + [\text{p53}]} - con + P_h \frac{[\text{p53-P}]}{(k_{dep} + [\text{p53-P}])} \\
&\quad - k_{1p}[\text{p53}][\text{Mdm2}] - k_{2p}[\text{p53}], \\
\frac{d[\text{p53-P}]}{dt} &= \frac{[\text{Atm-P}][\text{p53}]}{k_p + [\text{p53}]} + con - k_{p3}[\text{Mdm2}][\text{p53-P}] \\
&\quad - P_h \frac{[\text{p53-P}]}{(k_{dep} + [\text{p53-P}])} - k_d[\text{p53-P}], \\
\frac{d[\text{Mdm2-p53}]}{dt} &= k_{1p}[\text{p53}][\text{Mdm2}] - k_{c1}[\text{Mdm2-p53}], \\
\frac{d[\text{Mdm2-p53-P}]}{dt} &= k_{p3}[\text{p53-P}][\text{Mdm2}] - k_{c2}[\text{Mdm2-p53-P}],
\end{aligned}
\tag{3}
$$

$$
\begin{aligned}
\frac{d[\text{Mdm2}]}{dt} &= P_1 \frac{[\text{p53-P}]^4}{k_m + [\text{p53-P}]^4} - k_{1p}[\text{Mdm2}][\text{p53}] - k_{4a}[\text{Mdm2}][\text{Arf}] - k_5[\text{Mdm2}] \\
&\quad - k_{p3}[\text{Mdm2}][\text{p53-P}] + k_{c2}[\text{Mdm2-p53-P}] + k_{c1}[\text{Mdm2-p53}], \\
\frac{d[\text{Mdm2-Arf}]}{dt} &= k_{4a}[\text{Mdm2}][\text{Arf}] - k_6[\text{Mdm2-Arf}], \\
\frac{d[\text{Arf}]}{dt} &= p_0[\beta\text{-catenin}] - k_{4a}[\text{Mdm2}][\text{Arf}] - k_7[\text{Arf}] + k_6[\text{Mdm2-Arf}], \\
\frac{d[\text{Siah}]}{dt} &= p_3 \frac{[\text{p53-P}]^4}{k_s + [\text{p53-P}]^4} + k_{c3}[\beta\text{-catenin-Siah}] - k_{c4}[\beta\text{-catenin}][\text{Siah}] - k_{si}[\text{Siah}], \\
\frac{d[\beta\text{-catenin}]}{dt} &= p_{1p} - k_8[\beta\text{-catenin}] - k_{c4}[\beta\text{-catenin}][\text{Siah}], \\
\frac{d[\beta\text{-catenin-Siah}]}{dt} &= k_{c4}[\beta\text{-catenin}][\text{Siah}] - k_{c3}[\beta\text{-catenin-Siah}]
\end{aligned}
$$

The parameter values for these equations are given in supplementary materials. The transcriptionally active p53-P proteins form a tetramer [37], and hence the transcription rates

---

[3]Sionov, R.V., Hayon, I.L., & Haupt,Y.,(2000-2005) The regulation of p53 growth supression,http://www.ncbi.nlm.nih.gov/books/bv.fcgi?rid=eurekah.chapter.11736.

for MDM2 and ARF genes are described by a Hill coefficient of 4. The concentration of Atm-P, which determines the amount of phosphorylated p53, is treated as a parameter in these equations.

In Fig. 3A, we plot the steady state concentrations of p53-P as a function of the Atm-P concentration. p53-P exhibits oscillations for Atm-P > 0.22, i.e. in a region beyond the Hopf bifurcation. The kinetics for p53-P and Mdm2 concentrations, plotted in Fig. 3B for Atm-P $= 1$, show that they are out of phase with each other. p53-P is assumed to decay by two mechanisms: a first order decay that is independent of Mdm2 concentration, and another that is dependent on Mdm2 concentration. The second decay rate was assumed because without this critical assumption, the amplitudes of p53-P oscillations do not fall to low levels (supplementary material) as was observed in the experiment [18].

A sensitivity analysis shows that if the transcription rate of MDM2 is decreased, then this can be balanced by a slight increase in the transcription rate of SIAH, and vice versa. The decrease in SIAH transcription leads to a release of Mdm2 that was previously sequestered by Arf, and this counteracts the decrease in Mdm2. The control coefficients, $C_{P_1}^{\text{p53-P}}$, $C_{P_s}^{\text{p53-P}}$ are both negative, and are approximately of the same order of magnitude(see Supplementary materials). Increasing either of these two transcription rates leads to a decrease in p53-P, and hence they are mutually compensatory.

Integrated Model

The three modules are now combined into one integrated model. Eqs. 1, 2 and 3 are simulated with appropriate initial conditions to obtain the concentrations of the various species as a function of time. The initial conditions are the steady state concentrations of p53, p53-P, Mdm2, Arf, β-catenin, Siah, and the complexes. These steady state values are obtained by solving the rate equations for $S_D = 0$. The DNA breaks are assumed to occur at $t = 0$. Although the DNA breaks occur over a finite time interval, we assume that this is short

compared to the period over which repair occurs. The DNA damage turns the Atm switch **ON**, which rapidly makes Atm-P = 1, and Nbs1-P = 1 (see Fig. 2B). Since Atm-P > 0.22 (from Fig. 3A), the system crosses the Hopf Bifurcation point, and enters the oscillatory regime. p53-P begins to oscillate, and p53-P, Atm-P and Nbs1-P (through their respective actions not explicitly modelled here) begin to correct the damage (Eq. 1). As DNA repair proceeds, S_D decreases. At a certain threshold, Atm-P falls sharply back to its original value of zero (similarly for Nbs1-P). The Atm switch is shut **OFF**, and the system exits out of the oscillatory zone back to its original stable state. In Fig. 4A, we display the concentration of Atm-P, which rapidly rises to $\simeq 1$, remains at this value for a while, and finally rapidly declines as S_D decreases below a certain threshold. Also shown is the dynamics of p53 which falls from its steady state value close to $\simeq 2$, and oscillates with a small amplitude, but eventually rises to its original steady state value, as the repair is completed. All the other species described in Fig. 1 Module C also oscillate (i.e. Siah, β-catenin, Arf etc). In Figs. 4 (B-D), we plot the time series values of S_D, p53-P and Mdm2 for different initial values of DNA damage.

Note that the number of pulses increases with damage; however, the shape and frequency of the pulses do not change. This is consistent with the experimental observations that describe the "digital" behavior of p53 oscillations [18]. On DNA damage the system is moved into the oscillatory zone rapidly, by the Atm-P switch. Once inside the oscillatory zone, the switch is **ON** at a fixed value of Atm = 1, which fixes the amplitude of the oscillations. Similarly when the switch turns **OFF** the system moves out of the zone rapidly. Hence even though in this case the system exhibits a supercritical Hopf bifurcation, for which the amplitude of oscillations vary slowly with the value of Atm-P, the rapid movements into and out of the oscillatory regions give rise to fixed amplitude and frequency. An alternative model, as proposed in [22] is to employ a subcritical Hopf bifurcation which has the natural property to generate large amplitude oscillations with only small parameter changes.

Discussion

The model presented here describes the dynamics of a gene-regulatory network involved in DNA damage repair. We describe the model as three interacting modules. The p53, Mdm2, Siah, β-catenin, and Arf together represent the oscillator. The Atm, Nbs1 dynamics presents a switch. The repair process is active as long as p53-P, Atm-P and Nbs1-P are present. By modularizing the network we identified the key dynamical assertions (Fig. 1D). The Atm, Nbs1 switch is activated by DNA damage; the switch turns on Atm-P and p53 is phosphorylated; p53-P then begins to oscillate due to its interaction with Mdm2 (also through Arf, Siah, and β-catenin). The damage begins to be repaired because p53-P, Atm-P and Nbs1-P are abundant. The number of pulses of p53-P is proportional to the damage but the frequency and amplitude of the pulses remain the same. As S_D decreases the Atm-P activity is switched **OFF** and the system comes back to its steady state. Our model therefore supports a "digital" oscillatory behavior.

An important point is the sensitivity of the dynamics of the integrated model to parameter values. In Fig. 5 we plot on a logarithmic scale the range of parameter values for which the model exhibits qualitatively similar behavior.

There are a few critical parameters that determine the period and the amplitude of p53-P oscillations. Specifically, the rates of transcription of SIAH and ARF have significant effects on the period. This is intuitively obvious because these rates determine the rate at which Mdm2 is released from sequestration due to binding with the Arf protein. p53-P amplitude can be increased by changing the Michaelis-Menten constant that determines the rate of phosphorylation (i.e k_p). Similarly it can be decreased by increasing the transcription rate of MDM2 gene. These observations suggest simple tests. For example, partial functional knockout by siRNA could reduce the mRNA from any of the genes that form part of the p53 oscillator circuit. The model predicts that p53 oscillations would be affected by these partial knockouts.

The degradation of p53-P is a largely unknown process. If we only assume a simple first order rate of degradation proportional to p53-P the results of the simulations are inconsistent with experimental observation [18]. In particular the troughs in the oscillations of p53-P do not reflect the low levels observed in the experiment. To accommodate this discrepancy, we proposed an additional degradation route which is a function of both p53-P and Mdm2. Although the mechanism assumed here is similar to ubiquitination, there may be another mechanism though an intermediate gene product. With this addition to the model, the simulations faithfully reproduce the experimental observations. Experiments to test this alternative degradation routes should constitute removing Mdm2 and measuring p53-P degradation using antibodies specific to this isoform.

A crucial aspect of the model is the positive feedback regulation between Atm-P and Nbs1-P. This leads to a bistable switch-like model for the Atm activity. Here we have not explicitly modelled the mechanism of Atm activation by DSB, which may or may not require MRN. However, the positive feedback between Atm and Nbs1 is essential. Most recent in vivo experiments provide additional support for the positive feedback activation of Atm by Nbs1 [38]. To verify the Atm switch behavior, it is necessary to determine the two damage thresholds that occur in the bifurcation plot (Fig. 2A): The first is the minimum damage required to throw the Atm switch **ON** ($S_D \simeq 2.7$), and the second is the damage level at which the Atm switch turns **OFF** ($S_D \simeq 0.08$). The first threshold can be measured if cells are subjected to increasing doses of irradiation, and the damage level that turns Atm-P level **ON** is determined. Once the Atm switch is **ON**, we wait for the switch to turn **OFF** and at that point measure the existing DNA damage. The model predicts that the time taken to correct a larger amount of damage will be almost as long as that for a small amount of damage. This is because for high S_D, Atm-P levels are high and the repair progresses relatively rapidly, whereas for low S_D, the Atm switch is **OFF** and so correction must occur through basal amounts of Atm-P.

Transgenic mice with extra copies of p53 genes are resistant to tumor formation and age

normally, suggesting that increased doses of p53 gene may allow normal regulation [39]. By contrast, mice with a dominant negative form of p53 gene, whose product is always **ON** but is not subject to Mdm2 action, are radiation resistant but age faster. We predict that in these latter mice, p53 protein levels do not oscillate [40].

We note (Fig. 6, curve B) that by adjusting α and β (i.e., increasing the basal phosphorylation rates) it is possible to generate high levels of Atm-P even for a low S_D. By this analysis, if the basal rates of phosphorylation of Atm could be increased then the time taken to correct a small amount of damage could be decreased. This is testable by decreasing the concentrations of phosphatases through the use of siRNA. Furthermore, if k_0 is decreased, which corresponds to inefficient phosphatase binding to Atm, the steady state values of Atm-P for small S_D remain at a high level (Fig. 6, curve A). Therefore it would be instructive to examine the possible existence of cell lines where the levels of p53 naturally oscillate even in the absence of much DNA damage. We predict that, if such cell lines exist, mutations in these lines should affect the binding of phosphatases to Atm.

In this work we have neglected the effects of stochastic fluctuations in chemical species by assuming that the concentrations of all species are large. In a future publication we will examine the effects of stochastic noise on small concentration ranges.

Acknowledgement

References

[1] Vogelstein, V., Lane, D., & Levine, A.J. (2000) *Nature.* **408**, 307-310.

[2] Alarcon-Vargas, D., & Ronai, Z. (2002) *Carcinogenesis* **4**, 541-547.

[3] Malkin, D. (1994) *Ann. Rev. Genet.* **28**, 443-465.

[4] Harris, S.L.,& Levine, A.J. (2005) *Oncogene* **24**, 2899-2908.

[5] Oren, M. (2003) *Cell Death and Differentiation* **10**, 431-442.

[6] Lowe, S., Cepero,E., & Evan, G. (2004) *Nature* **432**, 307-315.

[7] Kohn, K.W., & Pommier, Y. (2005) *Biochem. and Biophys. Res. Comm.* **331**, 816-827.

[8] Matsuda, K., Yoshida, K., Taya, Y., Nakamura, K., Nakamura, Y., & Arakawa, H. (2002) *Cancer Research* **62**, 2883-2889.

[9] McKinnon,P.J. (2004) *EMBO reports* **5**, 772-776.

[10] Lee, J.H., & Paull, T. T. (2005) *Science* **22**, 551-554.

[11] Abraham,R.T. (2003) *BioEssays* **25**, 627-630.

[12] Bakkenist, C.J., & Kastan, M.B. (2003) *Nature* **421**, 499-505.

[13] Grossman, S.R., Deato, M.E., Brignone, C., Chan, H.M., Kung, A.L., Tagami, H., Nakatani, Y., & Livingston, D.M. (2003) *Science* **300**, 342-344.

[14] Paull, T.T., & Lee, J.H. (2005) *Cell Cycle.* **6**, 737-740.

[15] Lee, J.H., & Paull, T. T. (2004) *Science* **304**, 93-96.

[16] Buchhop, S., Gibson, M.K., Wang, X.W., Wagner, P., Sturzbecher, H.W., & Harris, C.C. (1997) *Nucleic Acids Res.* **19**, 3868-3674.

[17] Duensing, A., & Duensing, S. (2005) *Biochem Biophys Res Commun.* **3**, 694-700.

[18] Lahav, G., Rosenfeld, N., Sigal, A., Geva-Zatorsky, N., Levine, A.J., Elowitz, M.B., & Alon, U. (2004) *Nature* **36**, 147-150.

[19] Tyson, J.J. (2004) *Nature Genetics* **36**, 113-114.

[20] Strogatz, S. (1994) *Nonlinear Dynamics and Chaos:With Applications to Physics, Biology, Chemistry and Engineering* (Addison-Wesley, Reading, MA).

[21] Kuznetsov Y. A. (1995) *Elements of applied bifurcation theory* (Springer-Verlag, NY).

[22] Ciliberto, A., Novak, B., & Tyson, J.J. (2005) *Cell Cycle* **4**, 107-112.

[23] Mayo, L.D., & Donner, D.B. (2002) *TRENDS in Biochemical Sciences* **27**, 462-467.

[24] Monk, N.A.M. (2003) *Current Biology* **13**, 1409-1413.

[25] Bar-Or, R.L., Maya, R., Segel, L.A., Alon, U., Levine, A.J., & Oren,M. (2000) *Proc. Natl. Acad. Sci. USA* **97**, 11250-11255.

[26] Sauro, H.M., Hucka, M., Finney, A., Wellock, C., Bolouri, H., Doyle, J. & Kitano, H. (2003) *OMICS* **7**, 355-372.

[27] Sauro, H.M., (2000). *Animating the Cellular Map: Proceedings of the 9th International Meeting on BioThermoKinetics.*, eds. Hofmeyr, J.-H.S., Rohwer, J.M. & Snoep, J.L. (Stellenbosch University Press), pp. 221228.

[28] Wellock, C., Chickarmane, V. & Sauro, H.M. (2005) *Bioinformatics* **21**, 823-824.

[29] Chickarmane, V., Paladudgu, S.R., Bergmann, F. & Sauro, H.M. (2005) *Bioinformatics* **18**, 3688-3690.

[30] Doedel, E. J., (1981) *Congr. Numer.* **30**, 265384.

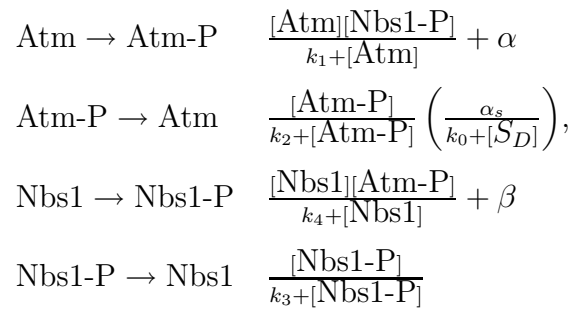[31] Sauro, H.M., & Kholodenko, B.N, (2004) *Prog. Biophys. Mol. Biol.* **86(1)** 5-43.

[32] Kurz, E.U., & Lees-Miller, S.P. (2004) *DNA Repair* **3**, 889-900.

[33] Goodarzi, A.A., Jonnalagadda, J.C., Douglas, P., Young, D., Ye, R., Moorhead, G.B., Lees-Miller, S.P., & Khanna, K.K. (2004) *The EMBO Journal* **22**, 4451-4461.

[34] Ferrell, J.E. (2002) *Curr. Opin. Cell. Biol.* **14**, 140-148.

[35] Ferrell, J.E., & Xiong, W. *Chaos* (2001) *Chaos* **14**, 227-336.

[36] Tyson, J.J., Chen, K.C., & Novak, B. (2003) *Curr. Opin. Cell. Biol.* **15**, 221-231.

[37] McLure, K.G., & Lee, P.W.K., (1998) *The EMBO Journal* **17**, 33423350.

[38] Difilippantonio, S., Celeste, A., Fernandez-Capetillo, O., Chen, H.T., Reina San Martin, B., Van Laethem, F., Yang, Y.P., Petukhova, G.V., Eckhaus, M. & Feigenbaum, L. *et al.* *Nature* (2005) **7**, 648-650.

[39] Garcia-Cao, I., Garcia-Cao, M., Martin-Caballero, J., Criado, L.M., Klatt, P., Flores, J.M., Weill, J.C., Blasco, M.A. & Serrano, M. (2002) *EMBO J.* **22**, 6225-6235.

[40] Tyner, S.D., Venkatachalam, S., Choi, J., Jones, S., Ghebranious, N., Igelmann, H., Lu, X., Soron, G., Cooper, B., Brayton, C., *et al.* (2002) *Nature* **6867**, 45-53.

Supplementary Materials

In this supplement we describe reaction schemes, parameter values, and supplementary figures referred to in the main manuscript.

Atm Switch Dynamics

The reaction scheme, from which Eq 2, in the main text, are derived is described by,

---

Atm $\rightarrow$ Atm-P	$\frac{[\text{Atm}][\text{Nbs1-P}]}{k_1+[\text{Atm}]} + \alpha$
Atm-P $\rightarrow$ Atm	$\frac{[\text{Atm-P}]}{k_2+[\text{Atm-P}]} \left(\frac{\alpha_s}{k_0+[S_D]} \right),$
Nbs1 $\rightarrow$ Nbs1-P	$\frac{[\text{Nbs1}][\text{Atm-P}]}{k_4+[\text{Nbs1}]} + \beta$
Nbs1-P $\rightarrow$ Nbs1	$\frac{[\text{Nbs1-P}]}{k_3+[\text{Nbs1-P}]}$

Reaction Scheme for the Atm Switch

The parameter values for these equations are reported in Table. 1. Each of Atm and Nbs1 are conserved cycles, i.e. Atm+Atm-P = 1, and Nbs1+Nbs1-P = 1

k_1	k_2	k_3	k_4	k_0	α	β	α_s
0.01	1	0.1	0.01	0.1	1E-4	1E-4	0.3

Table 1: Parameters used for the Atm switch.

In the model for the Atm switch, we assume a positive feedback, by allowing Nbs1-P to positively regulate the phosphorylation of Atm to Atm-P. Here we show though simulation, the effect of neglecting the positive feedback, on the dynamics of Atm-P. Although Atm-P levels rise rapidly with DNA damage, the decline with subsequent DNA repair, is slow, and hence

this would not explain the switch-like behavior of Atm-P. As is explained in the main text, the rapid drop in Atm-P levels is required to turn **OFF** the p53 oscillator.

If in the above reaction scheme, we leave out the positive feedback, in the activation of Atm-P by using Atm $\rightarrow$ Atm-P , with the rate law, $\frac{[\text{Atm}]}{k_{1p}+[\text{Atm}]} + \alpha$, then a simulation of the switch model leads to the results shown in Fig. 7. The dynamics of Atm-P does not rapidly decline as the damage decreases. The latter effect is required to turn off the p53 oscillator.

In the main text in Fig. 6, we show plots of the steady state values of Atm-P, as a function of S_D, for two cases. case A: Modified phosphatase activity, with $k_0 = 1$. case B: Increase in the basal phosphorylation rates, $\alpha = 0.01, \beta = 0.01$. The rest of parameters remain the same for both cases (as given in Table 1).

p53 Oscillator Dynamics

The equations for the p53 oscillator model given in Eq. 3, in the main text are obtained from the following reaction scheme,

$source \rightarrow \text{p53}$ $\qquad c_0$

$\text{p53} \rightarrow \text{p53-P}$ $\qquad \text{Atm-P}\dfrac{[\text{p53}]}{(k_p+[\text{p53}]}+con$

$\text{p53-P} \rightarrow \text{p53}$ $\qquad P_h\dfrac{[\text{p53-P}]}{(k_{dep}+[\text{p53-P}])}$

$\text{p53-P} \rightarrow sink$ $\qquad k_d[\text{p53-P}]$

$source \rightarrow \text{Mdm2}$ $\qquad P1\dfrac{[\text{p53-P}]^4}{(k_m+[\text{p53-P}]^4)}$

$\text{Mdm2} + \text{Arf} \rightarrow \text{Arf-Mdm2}$ $\qquad k_{4a}[\text{Mdm2}][\text{Arf}]$

$\text{Arf-Mdm2} \rightarrow sink + \text{Arf}$ $\qquad k_6[\text{Arf-Mdm2}]$

$\text{p53} + \text{Mdm2} \rightarrow \text{p53-Mdm2}$ $\qquad k_{1p}[\text{p53}][\text{Mdm2}]$

$\text{p53-Mdm2} \rightarrow \text{Mdm2} + sink$ $\qquad k_{c1}[\text{p53-Mdm2}]$

$\text{p53} \rightarrow sink$ $\qquad k_{2p}[\text{p53}]$

$source \rightarrow \beta\text{-catenin}$ $\qquad p_1$

$source \rightarrow \text{Siah}$ $\qquad Ps\dfrac{[\text{p53-P}]^4}{(k_s+[\text{p53-P}]^4)}$

$\text{Siah} + \beta\text{-catenin} \rightarrow \beta\text{-catenin-Siah}$ $\qquad k_{c4}[\text{Siah}][\beta\text{-catenin}]$

$\beta\text{-catenin-Siah} \rightarrow \text{Siah} + sink$ $\qquad k_{c3}[\beta\text{-catenin-Siah}]$

$\text{Arf} \rightarrow sink$ $\qquad k_7[\text{Arf}]$

$source \rightarrow \text{Arf}$ $\qquad Pb[\beta\text{-catenin}]$

$\text{Siah} \rightarrow sink$ $\qquad k_{si}[\text{Siah}]$

$\beta\text{-catenin} \rightarrow sink$ $\qquad k_8[\beta\text{-catenin}]$

$\text{p53-P} + \text{Mdm2} \rightarrow \text{p53-PMdm2}$ $\qquad k_{p3}[\text{p53-P}][\text{Mdm2}]$

$\text{p53-PMdm2} \rightarrow \text{Mdm2} + sink$ $\qquad k_{c2}[\text{p53-P}][\text{Mdm2}]$

$\text{Mdm2} \rightarrow sink$ $\qquad k_5[\text{Mdm2}]$

where the parameter values are given in Table 2, ,

k_{p3}	k_p	con	P_h	k_{dep}	k_d	k_{1p}	k_{2p}	k_{c1}	k_{c2}	P_1	k_m
0.005	0.4	1E-4	1E-6	1	0.006	1	0.5	1	1	0.4	1

k_5	k_{4a}	k_s	k_6	p_0	k_7	p_3	k_{c3}	k_{c4}	p_1	k_8	k_{si}
1E-4	15	1E+5	2	0.01	0.3	0.1	2	3	1	0.2	0.02

Table 2: Parameters used in the equations.

and where the constitutive rate of production of p53 is $c_0 = 0.8$. In Fig. 8A, we plot the bifurcation plot for the steady states of p53-P, as a function of Atm-P. There are two supercritical Hopf bifurcations, between which the system exhibits oscillations. Note however, that the minimum value of the p53-P oscillations do not tend to a low value, as is experimentally observed. The time series of the concentrations for p53, Mdm2 are displayed in Fig. 8B, for Atm-P $= 1.0$.

Sensitivity Analysis for module C

In a sensitivity analysis of a network, the control coefficients C_j^i are typically computed,

$$C_j^i = \frac{p_j}{S_i} \frac{\partial S_i}{\partial p_j} \tag{4}$$

where S_i, p_j are the species, and the parameters respectively. Hence C_j^i expresses a fractional change in a species value, as one of the parameters is changed. The coefficient could be positive, or negative, depending on whether a small increase in a parameter tends to increase or decrease a species level. The sensitivity is obtained by linearizing the system about a steady state. In the case of the oscillator module, the system oscillates about an unstable point. We fix the value of Atm-P $= 1$, for which the steady state can be computed. The computation is done using the sensitivity features in JDesigner. In the table below, we compute the control coefficients for a few important parameters for the oscillator network

(we display only those control coefficients that are either reasonably large, or are important for regulation) , module C, which describe the regulation that occurs. .

$C_{c_0}^{\text{p53-P}}$	$C_{\text{Atm-P}}^{\text{p53-P}}$	$C_{P_1}^{\text{p53-P}}$	$C_{P_s}^{\text{p53-P}}$	$C_{P_b}^{\text{p53-P}}$
0.16	0.15	-0.26	-0.24	0.26

Table 3: Control coefficients for some of the important regulatory steps in module C.

For example we see that $C_{c_0}^{\text{p53-P}}$ is positive, which is intuitively obvious, since the parameter c_0 determines the production of p53. The control coefficients $C_{P_1}^{\text{p53-P}}, C_{P_s}^{\text{p53-P}}$, are approximately of same order, and of the same sign. An increase in P_1, P_s represents an increase in the transcription of MDM2, SIAH genes, both of which lead to a reduction in p53-P. Hence a reduction in either transcription rate, can be compensated by an increase in the other. $C_{P_b}^{\text{p53-P}}$ is positive due to the following: an increase in P_b, leads to an increase in Arf, which sequesters more of Mdm2 and hence reduces the degradation of p53 which therefore increases the amount of phosphorylated p53.
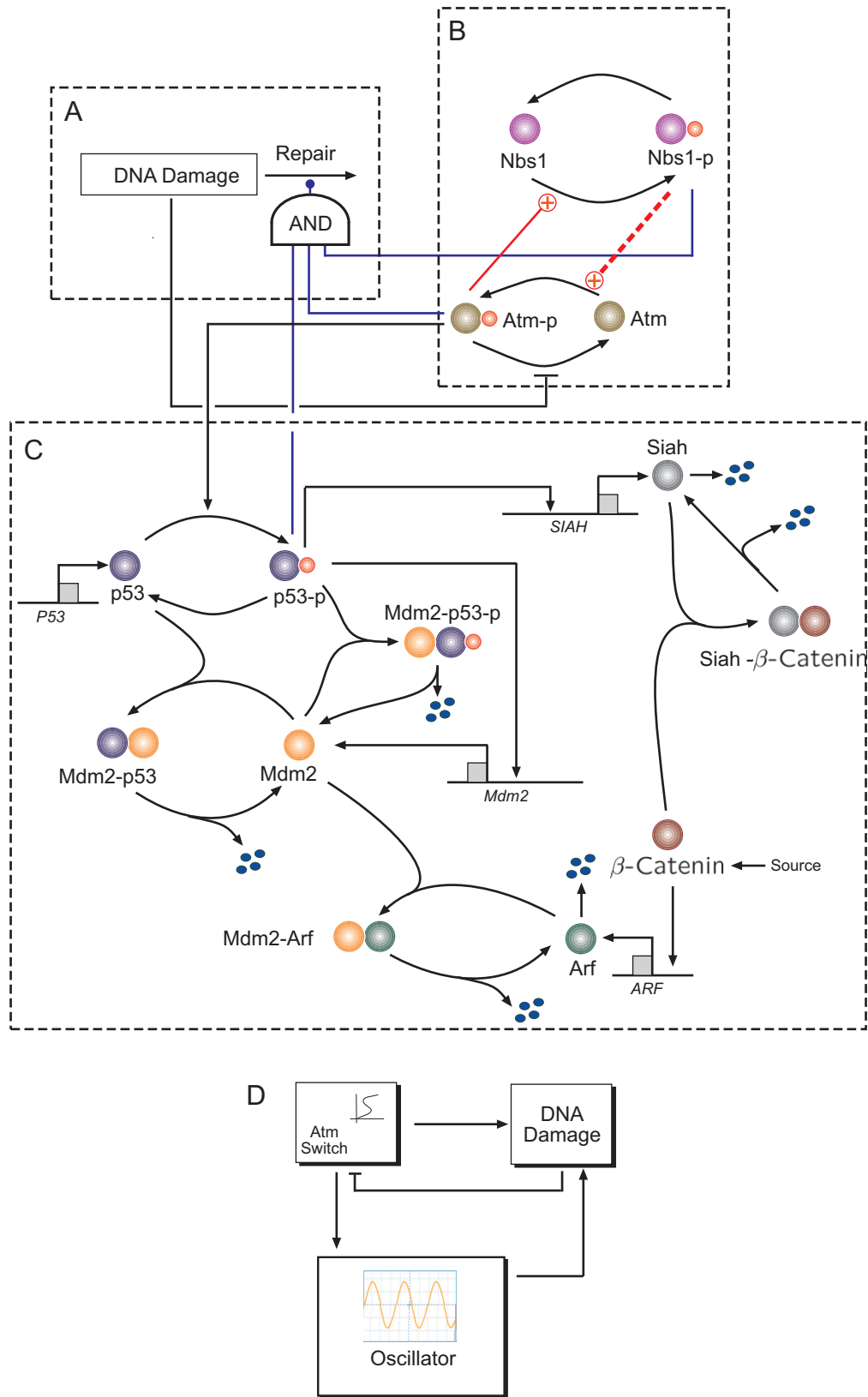
Figure 1: The core regulatory network. The three modules labeled as A, B and C, refer to the DNA damage repair, the Atm kinase switch, and the p53 oscillator respectively. These are described in detail in the text. Panel D presents a cartoon of the regulation for the integrated p53 network.
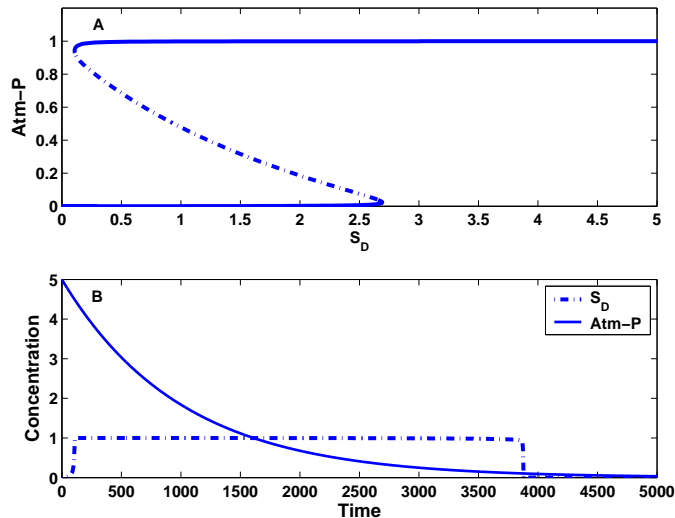
Figure 2: Bifurcation diagram and time series plot for the Atm kinase activity exhibiting bistability. The upper plot shows the steady state values of Atm-P as a function of the DNA damage signal S_D. The thick lines indicate the stable points, whereas the dotted lines indicate the unstable points. For $S_D > 2.7$, the system switches from a low value of Atm-P, to a high value of Atm-P (a similar bistable effect is observed for Nbs1-P). The lower plot shows the behavior of Atm-P as a function of time. In this simulation, S_D was modelled to be an exponentially decreasing function of time, and hence used as a parameter in Eq. 2. Initially the damage causes Atm-P to switch to a high level ($\simeq 1$), and then subsequently, as S_D decreases and crosses a certain threshold, the Atm-P switches back to a low value. The plot shows that as damage crosses $\simeq 0.08$, the switch is turned **OFF**, and one obtains a sharp crossover.
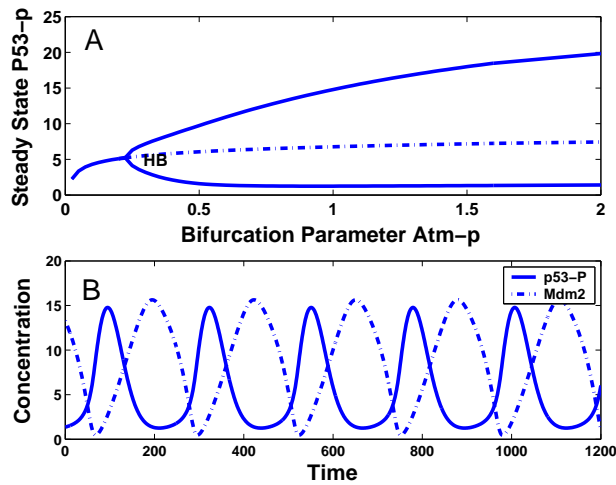
Figure 3: p53 and Mdm2 dynamics. Panel A shows the steady state value of p53-P as a function of Atm-P which shows a supercritical Hopf bifurcation (indicated by point HB) that occurs at Atm-P $\simeq$ 0.22. At this point the system develops stable oscillations, where the amplitudes of the oscillations increase with increasing Atm-P. The limits of the oscillations are marked by the thick lines. The dashed line after the point marked HB indicates the unstable branch. In panel B, we display the time series of p53-P and Mdm2, which can be seen to be out of phase. The overlap between the time series, occurs due to the activation-inhibition loop described in the model. For the plotted time series, the value of Atm-P = 1.0.
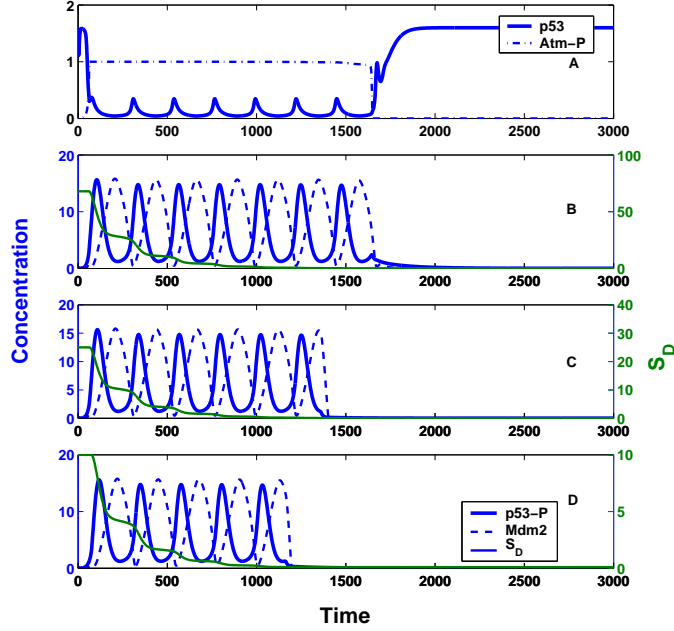
Figure 4: Effects of DNA breaks on p53 and Mdm2 dynamics. Panel A:Time-series plots for the concentrations of time courses for Atm-P and p53, for $S_D = 68$, at $t = 0$. Panels B-D:Time-series plots for p53-P, Mdm2 and S_D as a function of various initial damage levels, $S_D(t = 0) = 68, 25, 10$. The number of pulses increases with damage, while retaining their amplitude and frequency (in our model, the number of pulses is not a linear function of the damage. If however, we assume a Michaelis-Menten type of rate law for the damage such as assumed in [22], i.e the rate of change of damage is, $\propto -[\text{p53-P}]\frac{S_D}{k_{dam}+S_D}$, then for small k_{dam}, the rate of decay of damage(for $S_D > 1$) is proportional to the concentration of p53-P (since Nbs1-P, Atm-P$\simeq$ 1). From this it follows that the number of p53-P pulses required for repair will vary approximately linearly with respect to the amount of initial DNA damage.)
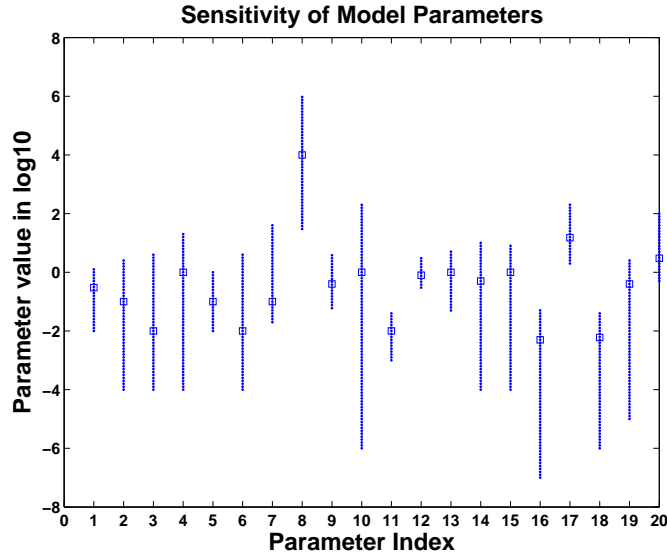
28

Figure 5: Sensitivity of model parameters to the system dynamics. A plot of the range of values of several parameters in logarithmic scale (base 10), vs the parameter index. The parameters are numbered from 1-20, and are listed below. The range (length of vertical line) indicates the set of values for which the system exhibits similar dynamics. The square symbol in each vertical line indicates the nominal value of the parameter in the model about which the range is computed. A short line segment indicates higher sensitivity to changes in the dynamics of the model, whereas a long line segment indicates robustness. For example, the model is very robust to changes in k_m (index 10), which is the Michaelis-Menten constant for the rate of production of Mdm2. Since the hill coefficient for this rate is 4, the transcription rate is fairly independent of the value of k_m. The model is sensitive to changes in c_0 (index 12), the rate of production of p53. The steady state concentration of p53 is relatively low in the cell, and this restricts the value of c_0 from assuming large values, whereas extremely low values of c_0 are insufficient to provide enough p53, p53-P to start the oscillations. The sensitivity plots were obtained by a combination of bifurcation studies and simulations for each of the following parameters in the same order as the "Parameter Index" in the figure. α, k_0, k_1, k_2, k_3, k_4, P_2, k_s, P_1, k_p, P_b, c_0, p_1, k_d, k_{1p}, k_{p3}, k_{4a}, k_d, k_p, k_{c4}
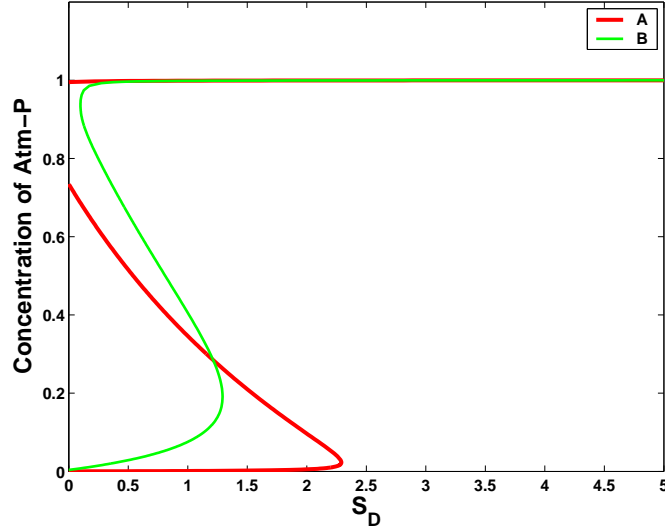
29

Figure 6: Bifurcation diagram for the steady state values of Atm-P as a function of S_D. Curve A: A bifurcation plot, for modified Phosphatase activity, which is obtained by changing k_0. The upper branch of the steady state values of Atm-P do not fall to zero, at low values of the DNA damage signal S_D, which means that as the damage is corrected the Atm switch is still in the **ON** state, and hence p53 oscillations continue even when damage is corrected. Curve B: The steady state values of Atm-P are reasonably higher at low values of the DNA damage signal S_D, as compared to a similar plot in Fig. 2, panel A. These higher basal rates of Atm-P and Nbs1-P would lead to faster DNA repair, for the same amount of small DNA damage, when compared to the case considered in Fig. 2, panel A. This plot has been obtained by increasing the values of α, β which corresponds to higher basal levels of phosphorylation (see supplementary materials for parameter values)
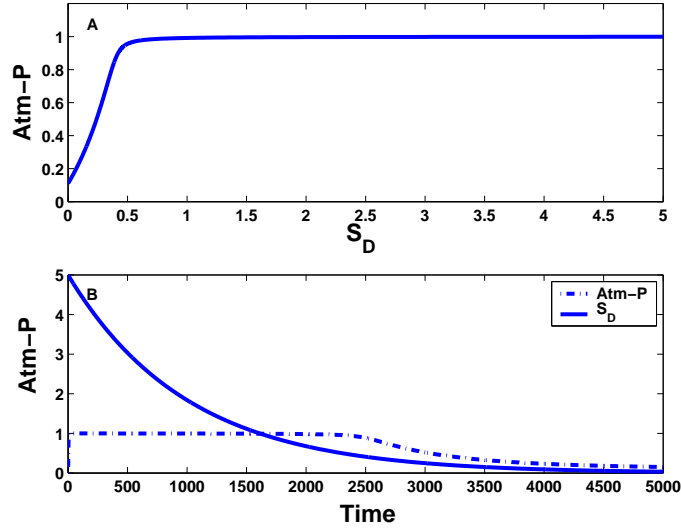
Figure 7: In the upper plot is shown the steady state values of Atm-P as a function of the DNA damage signal S_D, which shows ultrasensitive behavior. The lower plot shows Atm-P as a function of time. S_D, whose initial value is $S_D = 5$, is modeled here, as an exponentially decreasing function in time. Initially, Atm-P jumps almost immediately to a high level ($\simeq 1$), and then subsequently, as S_D decreases it reduces to a low value, but not rapidly enough, as is required by the integrated model.
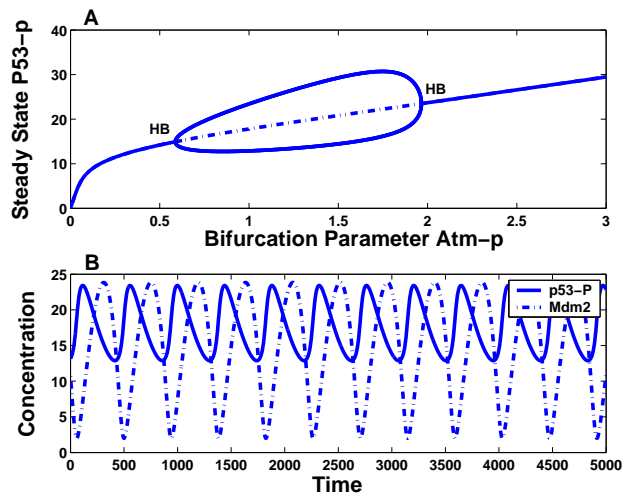

Figure 8: Panel A shows the steady state value of p53-P as a function of Atm-P which shows two supercritical Hopf bifurcations (indicated by point HB) that occurs at Atm-P $\simeq 0.6, 2.0$. Within this region, the system develops stable oscillations. The limits of the oscillations are marked by the thick lines. The dashed line between the points marked HB indicate the unstable branch. In panel B, we display the time series of p53-P and Mdm2 , for a value of Atm-P $= 1.0$.

31